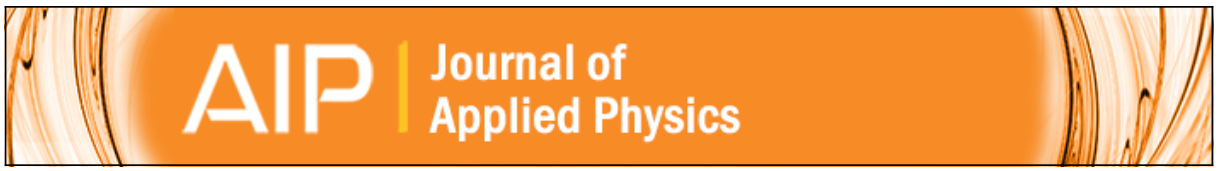

Annealing effects of Au nanoparticles on the surface-plasmon enhanced p-Si/n-ZnO nanorods heterojunction photodetectors

J. D. Hwang, F. H. Wang, C. Y. Kung, M. J. Lai, and M. C. Chan

Citation: Journal of Applied Physics **115**, 173110 (2014); doi: 10.1063/1.4875657
View online: http://dx.doi.org/10.1063/1.4875657
View Table of Contents: http://scitation.aip.org/content/aip/journal/jap/115/17?ver=pdfcov
Published by the AIP Publishing

Annealing effects of Au nanoparticles on the surface-plasmon enhanced p-Si/n-ZnO nanorods heterojunction photodetectors

J. D. Hwang,[1,a)] F. H. Wang,[2] C. Y. Kung,[2] M. J. Lai,[1] and M. C. Chan[2]
[1]*Department of Electrophysics, National Chiayi University, No. 300 Syuefu Rd., Chiayi City 60004, Taiwan*
[2]*Department of Electrical Engineering, National Chung Hsing University, No. 250 Kuo Kuang Rd., Taichung 402, Taiwan*

(Received 17 March 2014; accepted 28 April 2014; published online 7 May 2014)

The effects of various annealing temperatures (350–550 °C) of Au nanoparticles (NPs) on the surface-plasmon enhanced p-Si/n-ZnO nanorods (NRs) heterojunction photodetectors (HPDs) have been investigated. The photoresponse of the surface-plasmon-mediated HPDs was found to be determined by the extinction band of the Au NPs, the defects of ZnO NRs, and the Schottky-barrier height (SBH) between the Au and ZnO interface. The higher annealing temperature (550 °C) causes more defects in ZnO NRs and lowers the ultraviolet (UV) response of the fabricated p-Si/n-ZnO NRs HPDs. The higher annealing temperature also renders a rougher surface in the Au NPs, thereby leading to destructive interference and hence the narrowest extinction band. In contrast, the modest temperature (450 °C) results in fewer defects in ZnO NRs, the widest extinction band in Au NPs, and the lowest SBH at the Au/ZnO interface. Such a result enhances the UV-to-visible rejection ratio from 439.6 to 6447 as compared to the HPDs without Au NPs. A band diagram considering the above investigations is illustrated to elucidate the surface plasmon resonance effects on enhancing the UV response. © *2014 AIP Publishing LLC*.
[http://dx.doi.org/10.1063/1.4875657]

I. INTRODUCTION

With the progress in semiconductor technology, various opto-electronic semiconductor devices have been developed to the industry and commercial applications, such as Si,[1] Ge,[2] InGaAs,[3] GaN,[4–6] ZnO,[7–10] and CdS[11–13] based photodetectors (PDs), Si[14] and GaN[15] based light-emitting diodes (LEDs), as well as Si based solar cell.[16] Recently, surface plasmon resonance has been employed to increase their performance or efficiency because it allows the coupling of more light into or out of the devices.[17–19] The surface plasmon resonance, arising from the metal nanoparticles (NPs)/semiconductor interfaces, is currently being exploited due to its large light trapping and its enhancement in optical field. When the electromagnetic radiation illuminates the metal NPs, it can excite the localized plasma resonances within the particle layer, thereby inducing dipole oscillations in the individual particles, which will enhance the incident electromagnetic field near the particle by orders of magnitude, which will then couple radiatively with the semiconductor layer. The resonant frequency is determined by the various metals, the particle's size, shape, local dielectric environment, and it also covers large-scale optical regions, extending from the near ultraviolet (UV) through the visible range to the near infrared, thus leading to selective photon absorption and the local enhancement of the electromagnetic field.[17,18] This provides the possibility of controllably tuning the resonance wavelength, making the metal NPs very important and promising for a wide range of applications in the opto-electronic devices.[1–19] For these applications, their performance or efficiency all depend on the absorption range of the metal NPs and semiconductor characteristics, and the interface between the metal and the semiconductor. So a detailed study considering these issues is required.

In this work, a 4-nm thick Au film was deposited on the ZnO nanorods (NRs), which were then annealed at various temperatures to form Au nanoparticles. The effects of the various annealing temperatures on the enhancement of the UV response of the p-Si/n-ZnO NRs heterojunction PDs (HPDs) were investigated. It was found that the UV response was determined by the absorption band of Au NPs, the defects of ZnO NRs, and the Schottky-barrier height (SBH) between Au and ZnO interface. Various annealing temperatures in Au NPs lead to different behaviors in these issues and hence contributing UV response. The modest annealing temperature (450 °C) leads to a wider absorption band in Au NPs, with fewer defects in ZnO, and a lower SBH at the Au/ZnO interface. Based on these issues, the UV (340 nm)-to-visible (550 nm) rejection ratio is enhanced from 439.6 to 6447, as compared to the HPDs without Au NPs.

II. EXPERIMENTS

A (100) p-type silicon substrate with a resistivity in the range of 5–10 Ω cm was cleaned and the ZnO NRs were grown on the Si substrate by the hydrothermal (HT) method.[20] The aqueous solutions of zinc nitrate hexahydrate [$Zn(NO_3)_2{\cdot}6H_2O$, 0.05M] and hexamethylenetetramine ($C_6H_{12}N_4$, 0.05M) were mixed in a Pyrex glass bottle. Then, the substrates were dipped in the mixture for 40 min at 90 °C to prepare a ZnO seed-layer. Next, the annealing process was performed at 450 °C for 10 min in a N_2 atmosphere. The same mixed solution was used to grow ZnO NRs for 3 h at

a)Author to whom correspondence should be addressed. Electronic mail: jundar@mail.ncyu.edu.tw

90 °C. After that, a 4-nm thick Au film was deposited on the ZnO NRs, and then it was annealed under various temperatures (350, 450, and 550 °C) in vacuum. After the thermal annealing, the continuous Au film was broken into small nanoparticles due to the difference in the thermal expansion coefficients of Au and ZnO. Subsequently, a polymethyl methacrylate (PMMA) layer was placed between the ZnO NRs, in order to prevent the top Al electrodes from coming into contact with the Si substrate. The conductive Al electrodes were evaporated onto the ZnO surface and the backside of Si in order to form Ohmic contacts. The schematic structure of the fabricated p-Si/n-ZnO NRs HPD with the covering of Au NPs is illustrated in Fig. 1. Photoluminescence (PL) and scanning electron microscopy (SEM) were used to study the characteristics of the ZnO NRs with various temperatures annealing Au NPs. Morphology and extinction wavelength of Au NPs with various annealing temperatures were investigated by using atomic-force microscopy (AFM) and UV-visible measurement, respectively. The current-voltage (*I-V*) and photocurrent responsivity were used to measure the electro-optical properties of the fabricated p-Si/n-ZnO NRs HPDs with these Au NPs.

III. RESULTS AND DISCUSSION

The SEM image of the grown ZnO NRs with a cover of 350 °C annealed Au NPs is shown in the inset of Fig. 2. The ZnO NRs, grown by the HT method, appears as a hexagonal shape with a length of about 1.55 μm and a diameter ranging from 680 to 960 nm. It is clear that the top and the sidewall surfaces of the ZnO NRs are covered with Au NPs, which reveal non-regular shapes. With the rise in annealing temperature from 350 to 550 °C, the grain size of the Au NPs increase from 33 to 66 nm. The AFM measurement was employed by depositing a 4-nm thick Au film on the glass substrate and was annealed under 350–550 °C in vacuum. It appears that the surface roughness of the as-deposited Au film is 1.86 nm and increases to 3.64, 3.66, and 4.24 nm for the increased annealing temperature of 350, 450, and 550 °C, respectively. The increased grain size and the roughness

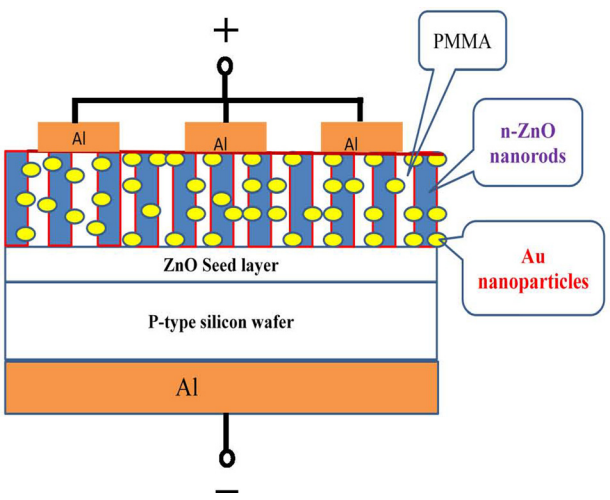

FIG. 1. Schematic structure of the fabricated p-Si/n-ZnO NRs HPD with the cover of Au NPs.

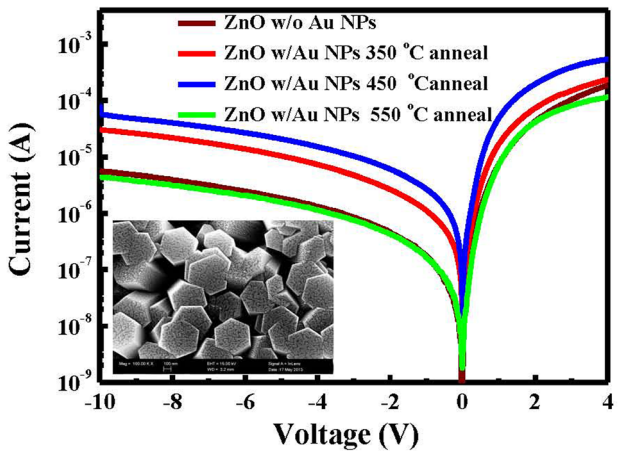

FIG. 2. Dark *I-V* characteristics of the fabricated p-Si/n-ZnO NRs HPDs with the Au NPs annealed under various temperatures. Also the HPD without Au covering is also compared. The inset is the SEM image of the grown ZnO NRs with 350 °C annealed Au NPs covering.

with the rise in annealing temperature are due to the agglomeration of the surrounding Au thin film. Theoretical investigations showed that the optical properties of metal NPs are dependent on the size and shapes, hence the non-regular shapes and grain sizes in the Au NPs determine the broadband plasmon resonance wavelengths.[21] The dark *I-V* characteristics of the fabricated p-Si/n-ZnO NRs HPDs with (w/) Au NPs annealed under various temperatures are shown in Fig. 2; the HPDs without (w/o) Au covering are also compared. Observable rectifying behavior appears in these HPDs, and the leakage current rises with the increase in annealing temperature. This occurs because the Au NPs can passivate the surface states of the ZnO NRs, and hence there are fewer O_2 and H_2O gas molecules being adsorbed; thus, fewer negative ions will form on the ZnO surface by trapping the free electrons in the film, i.e., $O_2(g) + e^- \rightarrow O_2^-$ and $2H_2O(g) + O_2 + 4e^- \rightarrow 4OH^-$. The fewer negative ions of O_2^- and OH^- will deplete fewer free electrons from the ZnO surface, resulting in small band bending near the surface and will easily make the electrons in the ZnO conduction band cross over the small built-in potential.[10] However, a drastic difference is observed in the HPDs with 550 °C annealed Au NPs, which reveals the lowest leakage current, thereby suggesting that more surface states existed on the ZnO surface. During the annealing of the Au film, the ZnO NRs also received the same annealing; where the high temperature annealing will degrade the ZnO quality and hence cause more surface states to arise due to the presence of porosity.[22]

The PL spectrum, shown in Fig. 3, was measured to investigate whether the 550 °C annealed ZnO NRs possess more defects than the ZnO NRs without annealing. From Fig. 3, all these ZnO NRs exhibit two emission bands of UV and visible, where the intensity of the visible band (450–700 nm) is amplified by 5 times. The UV light is emitted at 380 nm by the band-to-band recombination of ZnO. The visible band has broadband signals of deep-level emissions, which are generally attributed to the radiative recombination in the deep-level defects, where these deep-level defects originate from oxygen vacancies and zinc interstitial.[23] The PL intensity of UV (380 nm) and visible (550 nm)

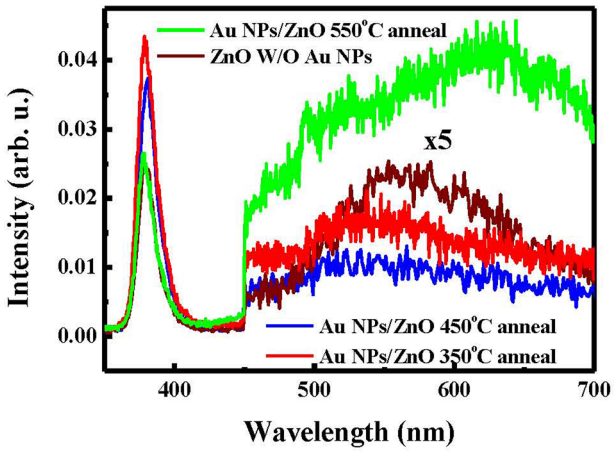

FIG. 3. PL spectrum for the ZnO NRs without and with Au NPs annealed at various temperatures.

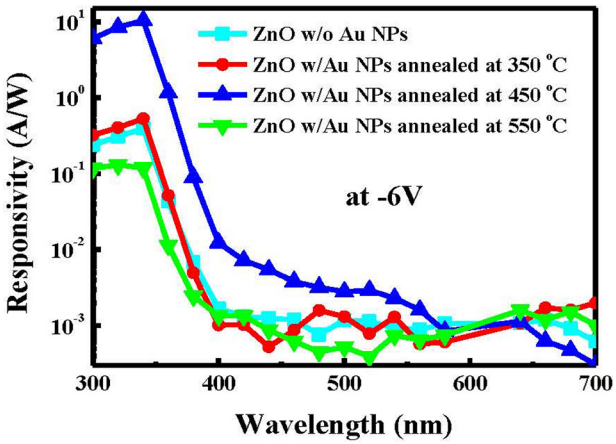

FIG. 4. Photocurrent responsivity versus various illumination wavelengths measured at 6-V reverse-bias voltage.

emissions, as well as the intensity ratio of 380 nm/550 nm, are listed in Table I. From the table, when compared to the ZnO NRs without Au NPs, the ZnO NRs with Au NPs demonstrate higher UV emissions for the 350 and 450 °C annealed ones, where the 350 °C annealed sample has a UV emission that is 1.79 times higher than the ZnO NRs without Au NPs. In contrast, the 550 °C annealed ZnO NRs presents a much lower UV emission than the 350 and 450 °C annealed ZnO NRs. Another interesting result is that the ZnO NRs, with 350 and 450 °C annealed Au NPs, reveal a lower visible response than the ZnO NRs without Au NPs. This indicates that the surface states of ZnO NRs are passivated for the 350 and 450 °C annealed samples; the obtained result is consistent with the above discussion. Conversely the ZnO NRs with 550 °C annealed Au NPs exhibit the largest visible response; where the visible response is even higher than the one without Au NPs, suggesting that the high annealing temperature indeed degrades the quality of the ZnO NRs, and hence leading to more defects. The highest ratio of UV (380 nm) to visible (550 nm) emission occurs in the ZnO NRs with 450 °C annealed Au NPs, where the ratio increases from 3.27 for a 550 °C annealed sample to 19.3 for the 450 °C annealed case by a magnitude of 5.9 times.

Photocurrent responsivity versus the various illumination wavelengths for these HPDs is presented in Fig. 4 under 6-V reverse-bias voltage. The responsivity reveals a sharp increase for a wavelength less than 380 nm, which is the band-edge absorption of ZnO and is consistent with the PL result. Clearly the HPDs with 350 and 450 °C annealed Au NPs possess higher UV responsivity (340 nm) than the HPDs without Au NPs. However, the HPDs with 550 °C annealed Au NPs appear the lowest UV responsivity, even lower than the one without Au NPs. The highest UV responsivity is achieved in the HPDs with 450 °C annealed Au NPs. These results are in good agreement with our prediction. It is worth noting that although the HPDs with 350 and 450 °C annealed Au NPs has 1 order of magnitude higher leakage current than the HPDs without Au NPs (see Fig. 2); however, their visible responses only show a slightly higher, or approximately the same values with the HPDs without the Au NPs. Such a result leads to the HPDs with 350 and 450 °C annealed Au NPs possessing a higher UV (340 nm)-to-visible (550 nm) rejection ratio. The ratio is only 439.6 for the HPDs without the Au NPs and increases to 921 and 6447 for the HPDs with 350 and 450 °C annealed Au NPs, respectively. As for the HPDs with 550 °C annealed Au NPs, the ratio is further reduced to 183 due to more defects. To study and obtain a clearer picture for the enhancement of the UV-to-visible rejection ratio, the 4 nm-thick Au was coated on a glass substrate and annealed at 350–550 °C; the extinction plot of the Au NPs on the glass substrate is shown in Fig. 5. A rather strong extinction band around the broadband signals of deep-level emission (450–700 nm) is found, indicating that the annealed Au NPs

TABLE I. The PL intensity of UV (380 nm) and visible (550 nm) emissions, as well as the intensity ratio of UV (380 nm)/visible (550 nm) emissions for the ZnO NRs without and with the Au NPs annealed under various temperatures.

	ZnOw/o Au NPs	ZnO w/Au NPs 350 °C anneal	ZnO w/Au NPs 450 °C anneal	ZnO w/Au NPs 550 °C anneal
380 nm	0.0239	0.0427	0.0367	0.0239
550 nm	0.0046	0.0035	0.0019	0.0073
380 nm/550 nm	5.19	12.2	19.3	3.27

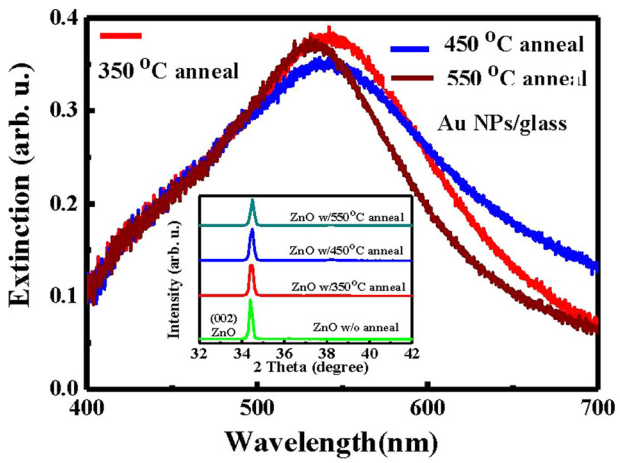

FIG. 5. Extinction plot of the Au NPs deposited on glass substrate and annealed at various temperatures. Inset is the X-ray diffraction patterns of the ZnO NRs grown on Si substrate with and without annealing.

have an effective absorption over the wavelengths of 450–700 nm. From the figure, the 450 °C annealed Au NPs demonstrates the widest extinction band; however, the narrowest extinction band is observed in the 550 °C annealed Au NPs due to the destructive interference on the rougher surface. X-ray diffraction patterns of the ZnO NRs grown on Si substrate with and without annealing are shown in the inset of Fig. 5. A preferred (002) peak appeared in these ZnO NRs, revealing they have highly c-axis-oriented structure. From the figure, the without annealing ZnO NRs demonstrates the narrowest full width at half maximum (FWHM), suggesting it possesses better crystalline than the others with annealing. The wider FWHM in the annealed ZnO NRs may be attributed that the thermal annealing degrades the crystalline structure.[20] However, from Fig. 3 of PL plot, the ZnO NRs, with 350 and 450 °C annealed Au NPs, reveal a lower visible response than the ZnO NRs without Au NPs. The result again confirms the Au NPs passivating the ZnO NRs surface.

The enhancement of the UV response in the fabricated HPDs is also related to the interface of the Au NPs/ZnO NRs, hence the *I-V* characteristics of the Au NPs/ZnO NRs annealed at various temperature is measured and shown in Fig. 6. All these curves present a clear rectifying behavior, indicating the characteristic between the annealed Au NPs and ZnO NRs is the Schottky diode. The SBH is estimated by the thermionic emission model[24] and shows the SBH to be 0.72, 0.67, and 0.70 eV for the annealing conditions of 350, 450, and 550 °C, respectively. This result demonstrates that the interface between the 450 °C annealed Au NPs and the ZnO NRs possess the lowest barrier height. From the above investigation, a band-diagram of Au NPs/n-ZnO NRs, shown in Fig. 7, is proposed to elucidate the enhancement of the UV response. The broadband emissions of the deep-level defects in ZnO (PL plot in Fig. 3) are absorbed by the Au NPs, which is denoted as process 1 in Fig. 7. Some of these emissions are scattered or reflected by the rough surface of the Au NPs, which are unavailable for contributing to the UV response. From Fig. 5, it can be seen that the 450 °C annealed Au NPs preserves the widest extinction broad band, hence it can absorb more defect-emissions through surface plasmon resonance due to the resonance energy of the Au

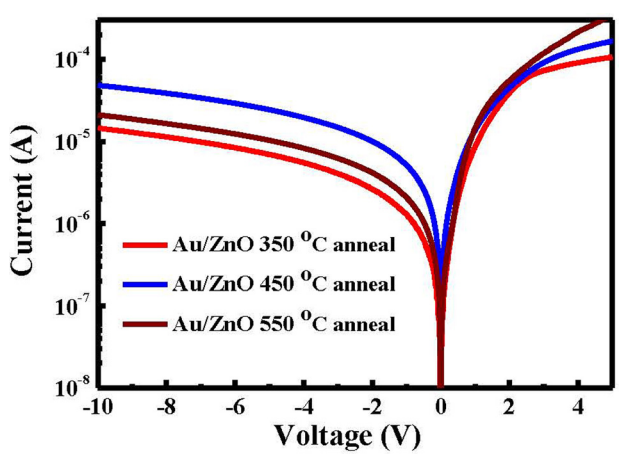

FIG. 6. *I-V* characteristic of the Au NPs/ZnO NRs Schottky diode with various annealing temperatures.

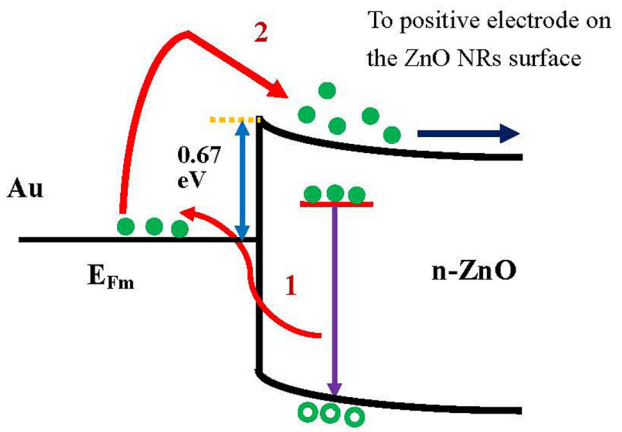

FIG. 7. Band-diagram of the Au NPs/n-ZnO NRs is proposed to elucidate the enhancement of the UV response.

NPs being close to the emission energy of deep-level defects (compare PL plot of Fig. 3 and extinction band of Fig. 5). The surface plasmon resonance will enhance the absorbed defect-emission near the Au NPs by orders of magnitude. Also the resonance energy of the Au NPs is within a range of 1.77–2.75 eV (corresponding to 450–700 nm), which is much higher than the barrier height of 0.67 eV between Au/ZnO interface for the 450 °C annealed one. Therefore, the enhanced emissions will excite the electrons in Au NPs to cross over the lower SBH and reach the ZnO side, denoted as process 2 in Fig. 7. The excitation transfers a great deal of electrons from the Au NPs to the conduction band of ZnO, and hence contributes to the UV response. Inspecting the responsivity of Fig. 4, no obvious reduction in visible response is seen although the visible emission is absorbed by the Au NPs. This is because the HPDs with Au NPs demonstrate higher leakage current at dark condition, shown in Fig. 2. Considering all the above discussions, the 450 °C Au NPs annealed HPD demonstrates fewer defect states in ZnO and the widest extinction band in Au NPs, as well as the lowest SBH in a NPs/ZnO NRs interface, hence it possesses the highest UV-to-visible rejection ratio. Photocurrent transient was measured on the 450 °C Au NPs annealed HPD by illuminating 366 nm UV-light at a reverse-bias voltage of 2 V. The photocurrent has an exponential dependence on the time, by fitting the curve and the response time was estimated to be 380 ms and 420 ms, respectively, for the rise and decay times.

IV. CONCLUSION

The effects of various annealing temperatures of Au NPs on the surface-plasmon enhanced p-Si/n-ZnO NRs HPDs have been investigated. The different annealing temperatures will vary the size and the shapes of the Au NPs, and in turn the extinction band. The widest extinction band occurs in the 450 °C annealed Au NPs; however, the higher annealing temperature (550 °C) results in the narrowest extinction band due to the destructive interference on the rougher surface. A higher annealing temperature degrades the ZnO NRs, thereby leading to more defects; in contrast, fewer defects are observed in the ZnO NRs with lower

annealing temperatures. The lowest SBH at the Au NPs/ZnO NRs interface is observed in the 450 °C annealed HPDs. Thus, the defect-emissions of the ZnO NRs are absorbed by the Au NPs and the emissions are enhanced due to the surface plasmon resonance between the Au NPs and ZnO NRs. The enhanced emissions excite a great deal of electrons crossing over the SBH and reaching ZnO NRs. Based on these investigations, the UV (340 nm)-to-visible (550 nm) rejection ratio is enhanced by 3.7 times in the HPDs with 450 °C annealed Au NPs as compared to the HPDs without Au NPs.

ACKNOWLEDGMENTS

This work was supported by the National Science Council of the Republic of China, Taiwan, under Contract No. NSC 102-2112-M-415-004-MY3.

[1]S. Y. Kim, C. H. Cho, B. H. Kim, Y. S. Choi, S. J. Park, K. Lee, and S. Im, Appl. Phys. Lett. **94**, 183108 (2009).
[2]F. F. Ren, K. W. Ang, J. Song, Q. Fang, M. Yu, G. Q. Lo, and D. L. Kwong, Appl. Phys. Lett. **97**, 091102 (2010).
[3]W. Wu, A. Bonakdar, and H. Mohseni, Appl. Phys. Lett. **96**, 161107 (2010).
[4]Z. D. Huang, W. Y. Weng, S. J. Chang, Y. F. Hua, C. J. Chiu, and T. Y. Tsai, IEEE Photon. Technol. Lett. **25**, 1809 (2013).
[5]K. Okamoto, I. Niki, and A. Scferer, Appl. Phys. Lett. **87**, 071102 (2005).
[6]J. D. Hwang and C. J. Lin, IEEE Electron Device Lett. **30**, 27 (2009).
[7]Z. S. Hu, F. Y. Hung, S. J. Chang, K. J. Chen, Y. W. Tseng, B. R. Huang, B. C. Lin, W. Y. Chou, and J. Chang, J. Nanopart. Res. **13**, 4757 (2011).
[8]D. Lin, H. Wu, W. Zhang, H. Li, and W. Pan, Appl. Phys. Lett. **94**, 172103 (2009).
[9]K. W. Liu, B. Liu, S. J. Wang., Z. P. Wei, T. Wu, C. X. Cong, Z. X. Shen, X. W. Sun, and H. D. Sun, J. Appl. Phys. **106**, 083110 (2009).
[10]H. K. Yadav, K. Sreenivas, and V. Gupta, Appl. Phys. Lett. **90**, 172113 (2007).
[11]K. Deng and L. Li, "CdS nanoscale photodetectors," Adv. Mater. (published online).
[12]L. Li, H. Lu, Z. Yang, L. Tong, Y. Bando, and D. Golberg, Adv. Mater. **25**, 1109 (2013).
[13]R. B. Konda, R. Mundle, H. Mustafa, O. Bamiduro, A. K. Pradhan, U. N. Roy, Y. Cui, and A. Burger, Appl. Phys. Lett. **91**, 191111 (2007).
[14]S. Pillai, K. R. Catchpole, T. Trupke, G. Zhang, J. Zhao, and M. A. Green, Appl. Phys. Lett. **88**, 161102 (2006).
[15]C. Y. Cho, S. J. Lee, J. H. Song, S. H. Hong, S. M. Lee, Y. H. Cho, and S. J. Park, Appl. Phys. Lett. **98**, 051106 (2011).
[16]J. D. Hwang and D. R. Hsieh, IEEE Electron Device Lett. **34**, 659 (2013).
[17]K. Wu, Y. Lu, H. He, J. Huang, B. Zhao, and Z. Ye, J. Appl. Phys. **110**, 023510 (2011).
[18]J. Song, X. An, J. Zhou, Y. Liu, W. Wang, X. Li, W. Lan, and E. Xie, Appl. Phys. Lett. **97**, 122103 (2010).
[19]A. J. Haes, S. J. Zou, G. C. Schatz, and R. P. V. Duyne, J. Phys. Chem. B **108**, 109 (2004).
[20]J. D. Hwang and Y. H. Chen, Thin Solid Films **520**, 5294 (2012).
[21]A. P. Abiyasa, S. F. Yu, S. P. Lau, E. S. P. Leong, and H. Y. Yang, Appl. Phys. Lett. **90**, 231106 (2007).
[22]Z. B. Fang, Z. J. Yan, Y. S. Tan, X. Q. Liu, and Y. Y. Wang, Appl. Surf. Sci. **241**, 303 (2005).
[23]H. Y. Lin, C. L. Cheng, Y. Y. Chou, L. L. Huang, and Y. F. Chen, Opt. Express **14**, 2372 (2006).
[24]J. D. Hwang, C. Y. Kung, and Y. L. Lin, IEEE Trans. Nanotechnol. **12**, 35 (2013).